

Experimental study of the effects of bio-inspired blades and 3D printing on the performance of a small propeller.

Christoph Hintz¹, and Pouria Khanbolouki²,

Department of Mechanical Engineering, University of New Mexico, Albuquerque, NM, 87131, U.S.A.

Andres M. Perez³,

Department of Mechanical Engineering, Universidad de Los Andes, Bogota, 111711, Colombia

and

Mehran Tehrani⁴, and Svetlana V. Poroseva⁵

Department of Mechanical Engineering, University of New Mexico, Albuquerque, NM, 87131, U.S.A.

The paper presents results of an experimental study conducted to understand the effect of a bio-inspired blade planform on the small propeller thrust and energy consumption. In the study, the Cicada wing was used as a prototype for the blade planform. This blade planform was combined with symmetric (NACA 0015) and asymmetric (NACA 64(4)-221) airfoils resulting in two propellers with bio-inspired blades. The comparative analysis of these two propellers is complimented with the analysis of two propellers with rectangular blades with the same profiles: NACA 0015 and NACA 64(4)-221. The two airfoils were selected for the study based on a review of airfoils suitable for small rotorcrafts, which are of interest for our research. The blade span and the blade planform area of the four propellers are the same. The propellers were manufactured using the 3D printing technology, which affects the blade shape and surface. A study was conducted to analyze the effect of 3D printing on the performance of the propellers with the NACA 0015 blade profiles. In the paper, the performance of propellers with untreated blades, that is, right after their printing, is compared with that of the same propellers, but with the blades soaked several times in a chemical solvent that smoothed the blade surface/shape.

I. Introduction

FLOWS around biological wings have been analyzed in many studies, with particular attention given to the analysis of a naturally moving wing such as a flapping wing, for example. Whereas the biological wing performance is optimal under such conditions, imitations of the natural flight may not necessarily be the optimal flight strategy from engineering perspective. Indeed, none of the existing successful flight strategies employed by our civilization relies on naturally moving wings. This may be due to the lack of knowledge and proper technologies or it may be relevant to our wish to fly higher, farther, and faster with heavier loads than naturally intended. In the latter case, naturally

¹Graduate student, UNM Electrical and Computer Engineering, 1 University of New Mexico MSC01 1100, Albuquerque, NM 87131.

²Graduate student, UNM Mechanical Engineering, 1 University of New Mexico MSC01 1150, Albuquerque, NM 87131.

³Graduate student, research was performed when visiting the Department of Mechanical Engineering, University of New Mexico, 1 University of New Mexico MSC01 1150, Albuquerque, NM 87131.

⁴Assistant Professor, UNM Mechanical Engineering, 1 University of New Mexico MSC01 1150, Albuquerque, NM 87131.

⁵Associate Professor, UNM Mechanical Engineering, 1 University of New Mexico MSC01 1150, Albuquerque, NM 87131, AIAA Associate Fellow.

moving wings may never quite work for our ambitions. Nevertheless, our belief is that some features of biological wings are of universal value, and our research goal is to identify such features and incorporate them in engineering technologies.

The focus of our current investigation is the insect wing shape and its potential use as a prototype for the rotor/propeller blade planform. Preliminary computational analysis of the flow structure around stationary and rotating Cicada wing-inspired blades conducted by our research group¹ demonstrated potential aerodynamic benefits of such a blade planform in comparison with a rectangular planform of the same span and area. Only very thin blades with a rectangular profile were considered in Ref. 1 to limit the analysis to the blade planform effects only. In particular, simulations demonstrated that size and strength of a vortex shed from the bio-inspired blade are reduced to compare with those of the vortex formed at the rectangular blade tip. Also, vorticity magnitude decreases more rapidly behind the bio-inspired blade. A level of the turbulent kinetic energy in the vortex behind the rectangular blade is higher than in the vortex behind the bio-inspired blade. Similar observations were made in a flow around rotating blades.

In Ref. 1, the Cicada wing was chosen as the blade prototype based on the thorough analysis of all insect orders^{1,2} with respect to the design features desirable in a small rotorcraft suitable for the use in residential areas. In this respect, there is no universal bio-prototype for the blade planform. Instead, its choice is driven by the blade application.

Due to proposed unusual use of bio-inspired blades, new experimental data are required to validate computational results. The goal of the current study is to conduct experimental analysis of thrust and energy consumption of propellers with the Cicada-inspired blades. Propellers have two blades with the Cicada-wing planform¹. The blades also have a lifting profile to enhance the blade lifting capability and to prevent early blade breaking at higher rotating speeds.

One of the objectives of our study is to investigate compatibility of the bio-inspired blade planform with an airfoil, symmetric or asymmetric. This is another step away from a natural wing. Two airfoils are used for this purpose: NACA 0015 (symmetric) and NACA 64(4)-221 (asymmetric) resulting in two blades and thus, two different propellers. The NACA 64(4)-221 airfoil was chosen following the general requirements for a rotorcraft airfoil: high maximum lift coefficient, high drag divergence Mach number, and good lift-to-drag ratio as well as low pitching moment³. The symmetric NACA 0015 airfoil is often used in blades of small helicopters.

Comparative analysis of thrust and energy consumption of the two propellers with bio-inspired blades at different rotating speeds is complimented with the analysis of two propellers with rectangular blades, but the same profiles (NACA 0015 and NACA 64(4)-221) as the bio-inspired blades. The blades of all four propellers have the same span and the same blade planform area.

Each propeller has been manufactured on the Dimension BST 1200es 3D printer as a whole unit with two blades rigidly attached to the propeller central part at the fixed pitch angle of 11° . CAD models for the propellers with the NACA 0015 profiles are shown in Fig. 1 as examples. 3D printing is a relatively new technology and although it facilitates the manufacturing process, it also affects the quality and shape of a design surface. These effects are not well understood, but are of importance for aerodynamic performance of propellers. This may be of particular importance for small propellers. Because studies are scarce (if any) in this area, one of our research objectives is to investigate how 3D printing affects propeller's thrust and energy consumption.

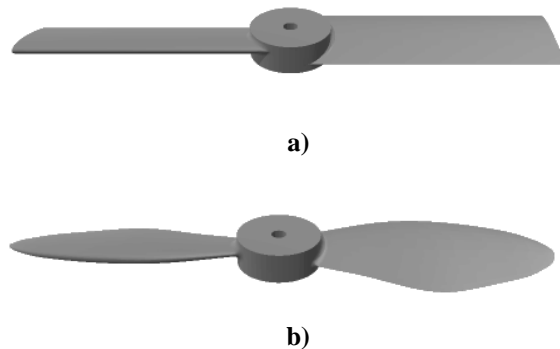


Figure 1. CAD models of the propellers with the NACA 0015 profile and a) rectangular and b) bio-inspired blade planforms.

II. Propellers

A. CAD Models

The starting point of designing propellers for this study was the bio-inspired blade planform from Ref. 1. The planform has the shape of an adult Cicada wing, with the maximum length in the span direction being 45.1 mm matching the size of the real Cicada wing. The chord size varies from 3.4 mm near the base of the wing (blade root), to a maximum of 17.5 mm matching the real wing dimensions. The surface area of the bio-inspired planform is 576 mm² as computed in SolidWorks.

The initial rectangular blade planform was designed to have the same span length and the same surface area as the Cicada wing, resulting in its chord length of 12.77 mm.

In the propeller blades, bio-inspired and rectangular blade planforms are combined with NACA 0015 and NACA 64(4)-221 airfoils resulting in four different blades. The blades were generated using the CAD package Solidworks.

The export wing files have been imported into software Autodesk Inventor which was used to design the propellers. Each propeller has two blades connected together by the cylinder-like section as shown in Fig. 1, which makes it possible to mount the propellers on the motor.

After initial attempts to manufacture and test propellers with blades that match exactly the insect wing dimensions, it was found necessary to enlarge the initial blade (and propeller) designs. All dimensions were enlarged proportionally, so that the final diameters of the propellers ($2R$) and the propeller hub ($2R_h$) are 23.12 cm and 35 mm, respectively. Because blades are fixed rigidly on the hub, the blade root smoothly envelops the hub, which makes the blade length from the blade root to its tip vary along the chord in all produced blades, with the shortest distance between the hub and the blade tip, R_b , being 9.81 cm in all blades. The chord of printed rectangular blades, c , is 32 mm. The hub thickness is 13 mm. All blades have the pitch angle of 11° to maximize the propeller thrust.

B. Manufacturing Procedure

The CAD models were converted to STL (stereolithography) files and manufactured with Acrylonitrile butadiene styrene (ABS-P430) through Fused Deposition Modeling (FDM) technology⁴. The material density is 1.04 g/cc. The 3D-printer used in this study is Stratasys⁵ model “Dimension BST 1200es” with two material cartridges and minimum layer thickness capability of 0.01 in (254 μ m). Higher layer thicknesses may result in better mechanical properties of a printed product due to lower effects from weakened inner layer adhesions. However, surface quality, shape of the propellers, and subsequently, the aerodynamic performance of them are the only concern of this study. So the minimum layer thickness was chosen to build the propellers for better conformity of the printed design to the curvatures from CAD model.

Three build orientations shown in Fig. 2 were taken into consideration to find the optimum direction for lowering the surface roughness. Other build directions would add layers of complexity in the symmetry of the blades regarding surface finish and geometry accuracy. The first build direction (Fig. 2a) shows perfect conformity with the airfoil perimeters, although the use of support material for overhangs under the propeller hub is unavoidable in this orientation and the support material would inevitably surround one of the blades, which eventually would affect the surface roughness of that blade. On the other hand, the second build direction (Fig. 2b) results in printing the hub with least defects, but the use of support material under the blades is also unavoidable. Additionally, large tangent angles of the airfoil cross-sections with vertical direction of the build orientation would result in the stairway effect and large cavities between the layers (Fig. 2b). The third build direction shown in Fig. 2c requires the least amount of support material and well adapts to symmetrical composition of the blades as well as to their pitch angle. Low tangent angles with the build direction are achieved in this case that allow one to avoid stairway effects. Additionally, sufficiently larger rasters in this direction in comparison to the first build direction shown in Fig. 2a minimize distortions in the direction of the blade span caused by the increased number of heating and cooling fluctuations of the stacked layers. It's noteworthy that smaller rasters may result in lower mechanical properties of the finished parts⁶. Consequently, the third build direction (Fig. 2c) was chosen for manufacturing all propellers in this study.

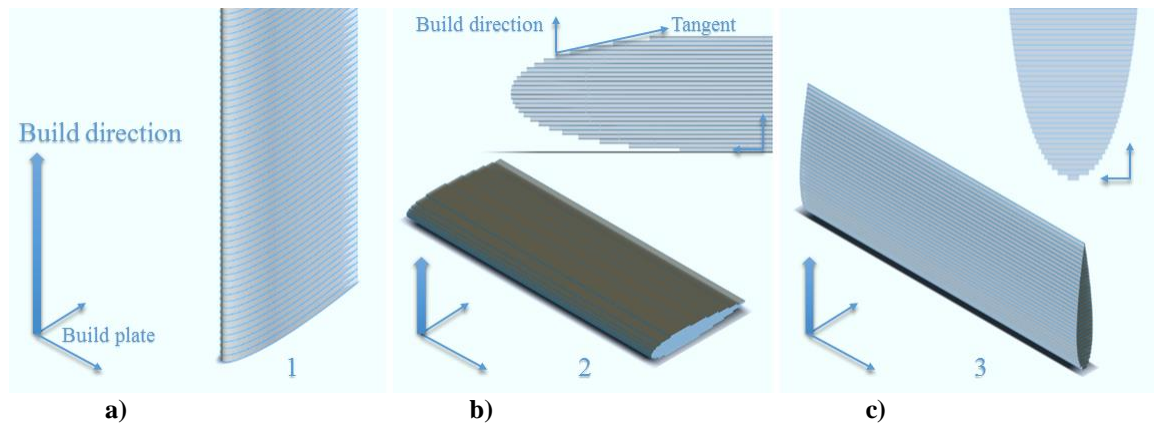


Figure 2. Schematics for the three build directions taken into consideration.

C. After-production Surface Treatment

Reduction of surface roughness of additively manufactured parts has been investigated to some degree with various methods such as subtractive manufacturing techniques⁷⁻⁹ and chemical treatments¹⁰. Chemical finishing processes either by vapors or immersion in solvents have shown to be effective methods for uniformly modifying the surface roughness of additively manufactured parts with minimum operator interference¹¹.

In the current study, a chemical bath is chosen for smoothing the blade surface of printed propellers for its low cost, availability, and high reaction rate. It has also been shown that chemical treatments have negligible effects on mechanical properties of 3D-printed ABS parts. Although, reduction of the surface roughness by dissolving the filaments is the most significant effect of this process¹².

Only propellers with the NACA 0015 profiles had been treated in the study with the purpose of improving their surface quality, that is, two out of the four manufactured propellers. This was determined from the experiments as discussed in the Results section.

The two propellers were post-treated in six consecutive steps in a bath of Dimethyl ketone (Acetone). The effective immersion time was determined in preliminary experiments where the same process was applied to dummy propellers with the same blade profiles and the same layer thickness builds. Because of the high diffusivity of acetone and low chemical resistance of ABS when in direct contact with acetone, a short period of 10 seconds was chosen for dipping process at each step to reduce damage to the structure of printed propellers. The propellers were dried overnight after each dipping step at room conditions. Experimental analysis of thrust and energy consumption of the propellers was performed prior to the first dipping of the propellers and then, repeated after each step of chemical treatment of the propellers.

The surface condition of treated propellers was documented in photographs. Figure 3 shows the surface of two propellers prior the chemical treatment. Improvement of the surface quality became observable from the second step of the treatment (after 20 seconds of immersion). Figures 4 and 5 show the bio-inspired propeller before the first treatment step, after 30 seconds of treatment, and after 60 seconds of treatment from different angles. The surface quality starts to deteriorate after 30 seconds of treatment. This can be seen in Figs. 4b,c and 5b,c as increased transparency of the blade thinner sections such as the trailing edge, for example, and in Fig. 5b,c as formation of grains on other areas of the blades.

In addition to the decreased surface roughness of the treated propellers due to removing edges of the deposited layers from 3D printing, dimensional changes were also observed after the chemical treatment. In particular, the hub height and diameter were reduced by the amounts of 0.003in and 0.006in, respectively, after six steps of the treatment; the rectangular blade chord had also a 0.006in reduction in length. The most significant reduction was observed in the thickness of the rectangular blade: ~0.08in.

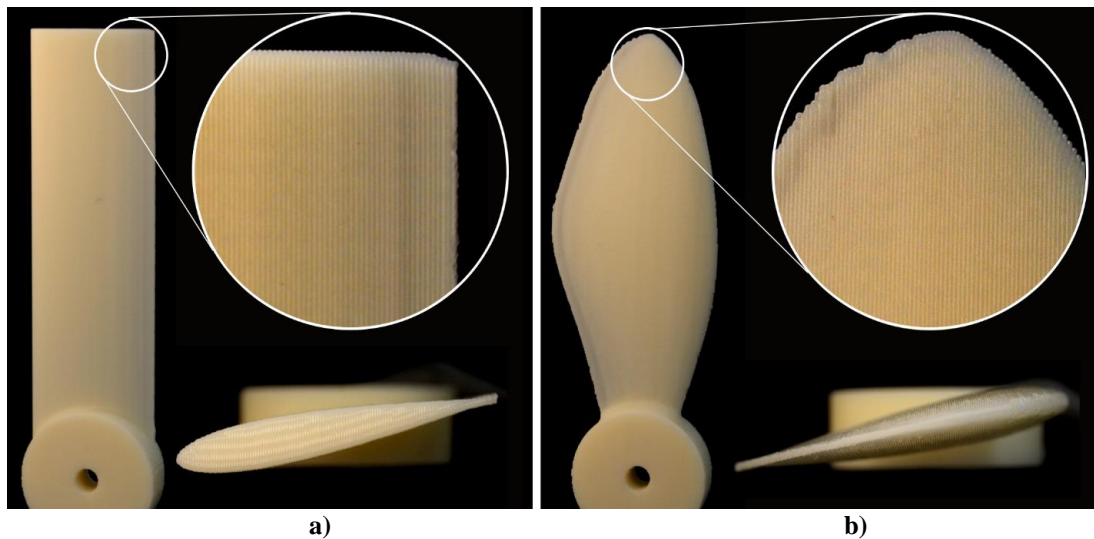


Figure 3. The printed propeller surface quality before the chemical treatment: a) rectangular blades, b) bio-inspired blades with the NACA 0015 profile.

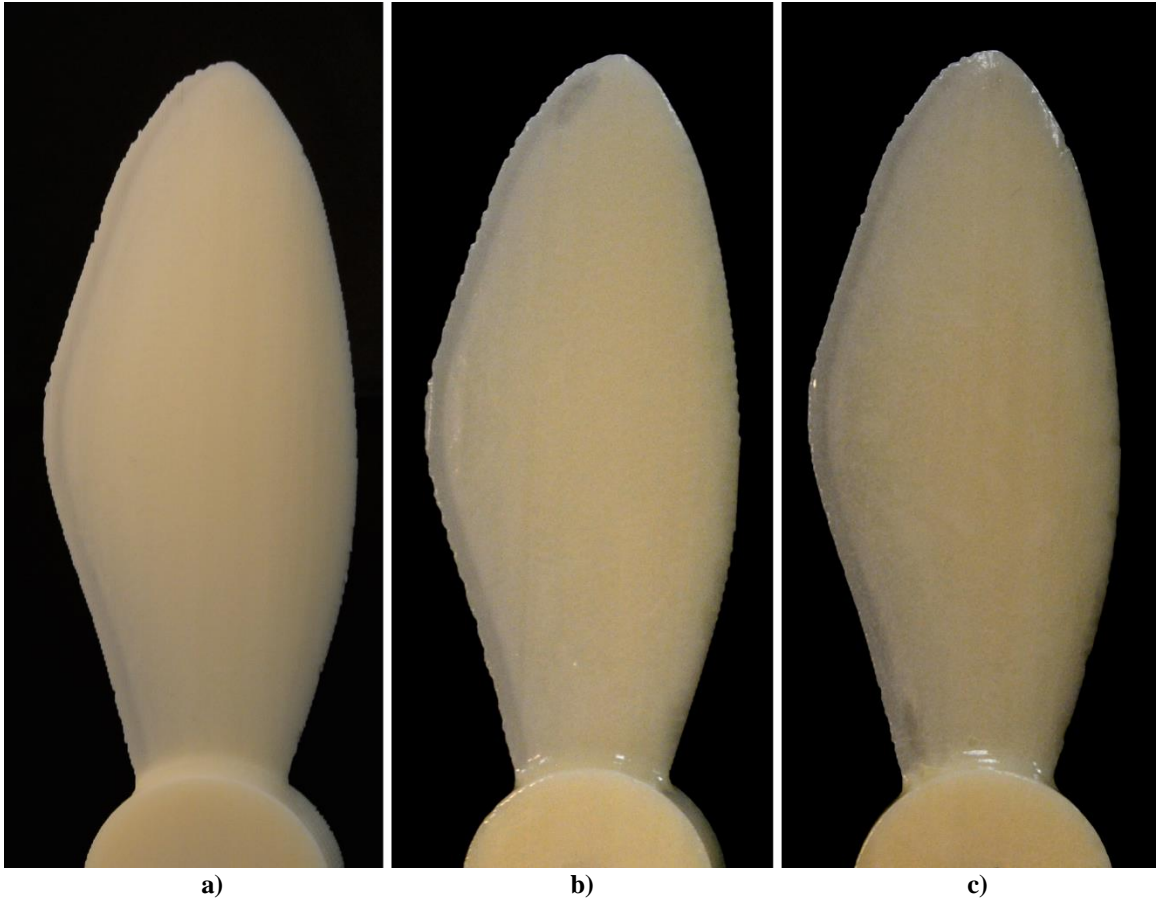


Figure 4. The surface quality of the propeller with bio-inspired blades with the NACA 0015 profile at different stages of the chemical treatment: a) before, b) after 30 sec, and c) after 60 sec.

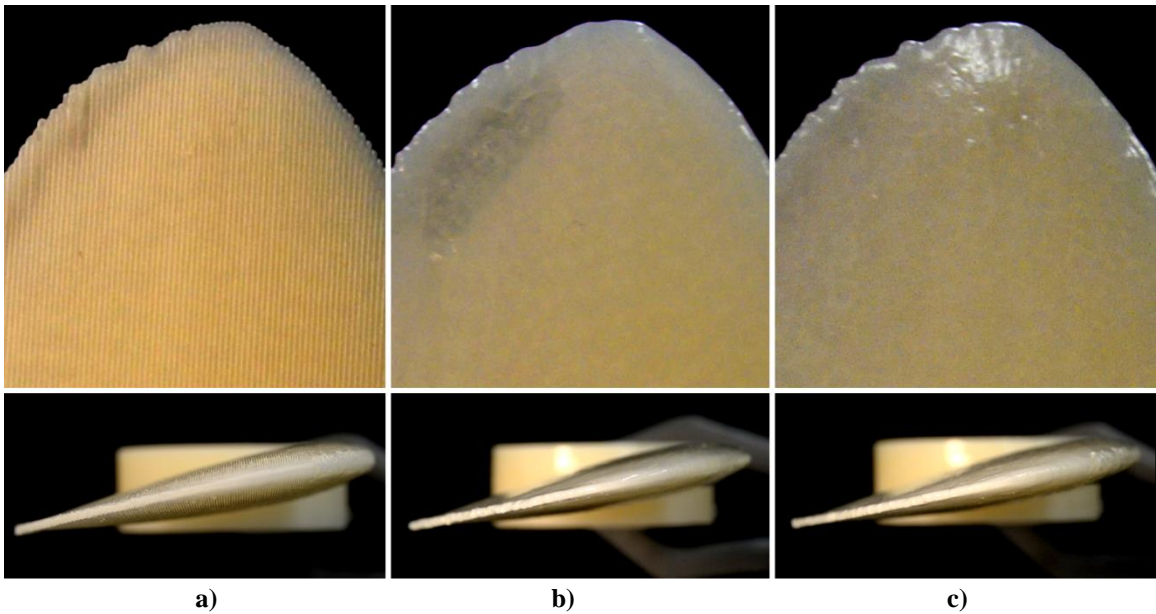


Figure 5. The near-tip surface quality of the bio-inspired blade with the NACA 0015 profile at different stages of the chemical treatment: a) before, b) after 30 sec, and c) after 60 sec.

III. Experimental Setup

A. Equipment

To test the performance of different propeller designs, a test stand was built at the Department of Mechanical Engineering, University of New Mexico, shown in Fig. 6. The experimental setup included the following components: 3D printed propellers, software Autodesk Inventor and SolidWorks, Turnigy Thrust Stand, Electronic Speed Controller (ESC) Plush 40A, 1460 kV brushless motor, Arduino Uno, AttoPilot voltage and current sensor, and 12V 10A Notebook charger as power supply.

The brushless motor used to run the experiments is a 1460 Kv brushless motor designed for radio control (RC) objects. The Kv rating means that its rotation speed is 1460 revolution per voltage applied in one minute if there is no load on the motor. It supports the maximum of 15 volts. A 40A Plush ESC is controlling the speed of the motor. For this experiment, a notebook charger which provides 12V is used as a power supply. It can provide up to 10A, which was important due to the high current draw of the motor at higher speeds. To measure the current, an AttoPilot voltage and current sensor measures the voltage and current between the power supply and the electronic speed controller.

The tool used to estimate the thrust of each propeller is a Turnigy thrust stand. The stand shows the thrust created by the propeller in gram-force, so that it is possible to convert the measurement to Newtons, where 1 gram-force represents 0.0098N. It can measure up to 5kg-force of thrust. It has high-precision linear bearings and thrust sensors to provide highly accurate results down to grams. The stand comes with the back light LED screen display for easy result reading.

An Arduino Uno control board is used to control the input voltage before it is supplied to the motor. Pulse-width-modulated (PWM) signals are sent by the control board to ESC, which can vary the voltage supplied to the motor accordingly. In parallel to the motor control, the Arduino gets supplied with the amps that are drawn by the motor with the help of the AttoPilot Sensor. This is a key point of the documentation so that in combination with the thrust stand the propellers can be characterized individually.

The voltage delivered from the DC power supply goes to ESC. ESC is a stand-alone unit, which provides an electronically generated three-phase electric power low voltage source of energy to the motor. It also converts the voltage from DC to AC.

Figure 7 shows a block diagram of the experimental setup used in the study with the connections between the components. The blue connections symbolize electronic wiring, the red connection is an electronic wiring that reads



Figure 6. Test stand.

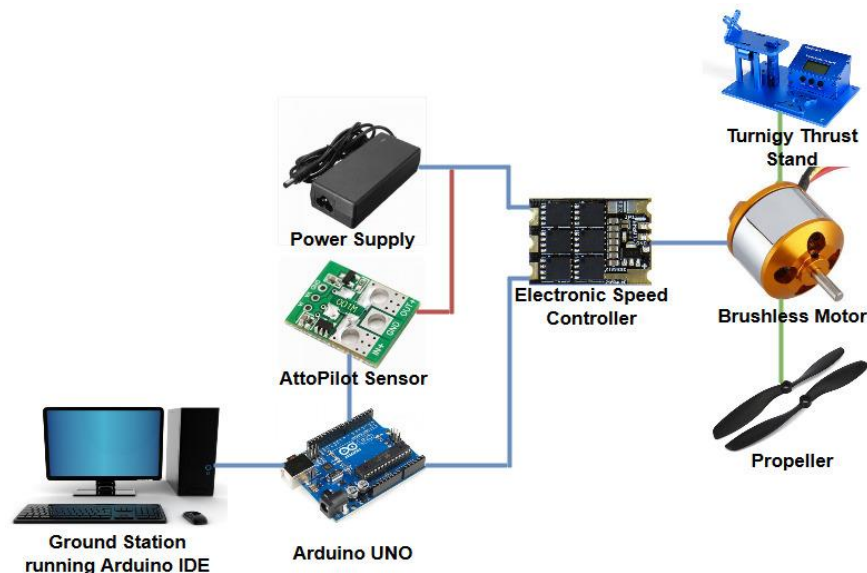


Figure 7. Schematic of the described setup

sensor data, and the green connection is established mechanically with screws and nuts. It can be noticed that the electronic speed controller has two voltage inputs, one from the power supply and the other from the Arduino Uno. The voltage supplied by the Arduino only acts as a signal line to control ESC. Voltage from the power supply is controlled by the electronic speed controller and ultimately, powers the motor.

Other equipment used in the study includes an EXTECH 461893 digital optical tachometer and a Fisher-Scientific XD400 electronic scale.

B. RC Motor Modeling

It is important to notice that there are three different outputs from the experiment. The first measurement is the thrust, T , (in gram-force) obtained from the Turnigy Thrust Stand, the second output is the voltage that is supplied to the motor by ESC, and the third output is the current drawn from the motor. This is the output that is the hardest to associate with aerodynamic characteristics of a blade.

To explain the relation between the mechanical torque needed to spin a blade and the current, a diagram of the circuit with the RC motor is shown in Fig. 8. In the figure, v represents the voltage supplied, R is the electric resistance, L is the electric inductance, i is the electric current, e is the voltage at the brushless motor, Q is the torque of the motor, θ is the rotational speed in RPM, and b is the motor viscous friction factor [13]. In the circuit, the torque is a linear function of the current:

$$Q = K_t \cdot i, \quad (1)$$

where K_t is motor torque constant. This relation shows that if the propeller spins at the same rotational speed, but it draws a different current, it can be related to the torque that the motor needs to rotate the propeller at the desired speed. This means that if there are two propellers with different blade designs that are tested with the same motor and with the same voltage supplied to the motor, a propeller that draws more current has blades that generate higher drag or/and lift forces.

The rotational speed required for the propeller performance analysis, was determined using two approaches in the present study. In one of them, its value was estimated from voltage, V , supplied to the motor, using a linear relation between them:

$$\theta = K_v \cdot V. \quad (2)$$

In the experiments, the rotational velocity calculated from (2) was varied in the range of 166 and 9000 RPM. At the lower limit of θ , a propeller starts to rotate. Safety concerns determined the upper limit.

The motor Kv rating characterizes the performance of a motor without a load. The load presence is likely to affect a relation between the rotational speed and voltage supplied to a motor. To estimate this effect, model (2) was validated against direct measurements of the rotational speed with the digital optical tachometer.

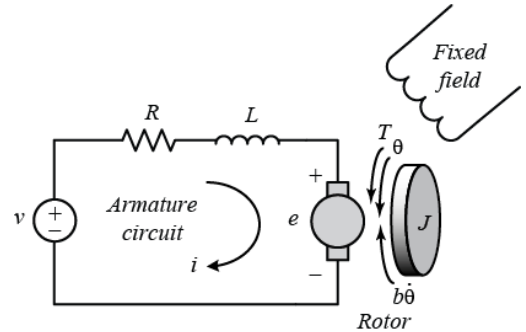


Figure 8. Armature circuit diagram for the brushless motor used in the experiment.

IV. Results

In the experiments, a control input from an operator is the rotational velocity value from model (2), which activates the motor, and can be increased or reduced incrementally with a prescribed step. Before analyzing the propeller performance, errors associated with the thrust measurements and with model (2) were investigated.

A. Modeling and Measurement Errors

To determine the accuracy of conducted thrust measurements, the test stand calibration was performed using calibrated weights. As the first step of the calibration procedure, the applied weight was gradually increased from 0.1N up to 15N and then, reduced back to 0.1N. The procedure was repeated 20 times, with the weight measurements from the test stand being collected for each applied load. The error of measurements was calculated as the percentage of the difference between applied and measured loads. Uncertainty in the collected data was calculated as the standard

deviation of the measurements. Figure 9 shows the results of the calibration process. The maximum error in the measurements was 8.36% for a load of 0.78N (79.6 gr), the maximum uncertainty was ± 13.63 gr for the applied load of 1244 gr.

To validate model (2) for the rotational velocity, several tests with different propellers were conducted where the rotational velocity obtained from (2) was compared against the rotational velocity obtained from direct measurements of this parameter using the digital optical tachometer. Results of the comparison for the propeller with rectangular blades, which have the NACA0015 profile are shown in Fig. 10. The figure demonstrates that in a presence of a load, model (2) tends to underestimate the rotational velocity values at lower velocities and underestimates this parameter at higher velocities.

Results for other tested propellers were similar, but the exact relation between predicted and measured rotational velocities depends on a load. In our measurements, a load (propeller mass) was 34gr (for a propeller with bio-inspired blades) and 31gr (for one with rectangular blades).

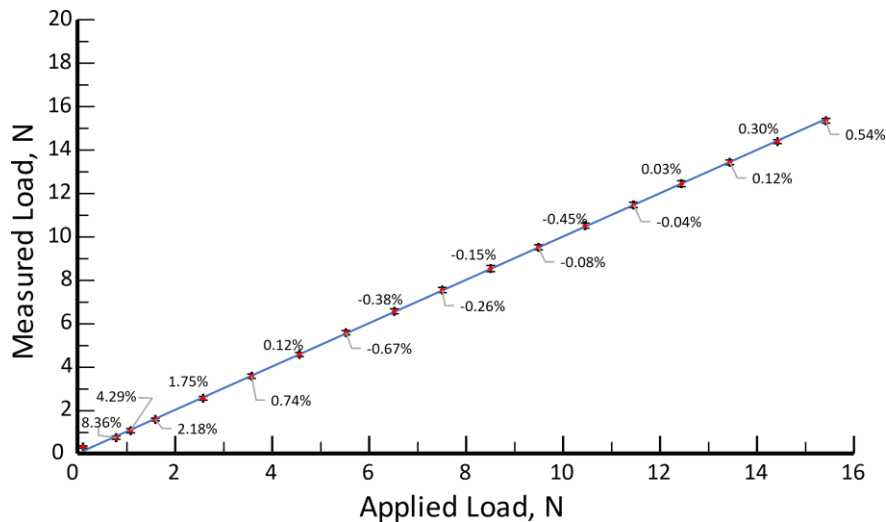


Figure 9. Results of the test stand calibration. Notations: average data are red points; expected measurements are shown by the blue line; and the numbers are the error of the measurements.

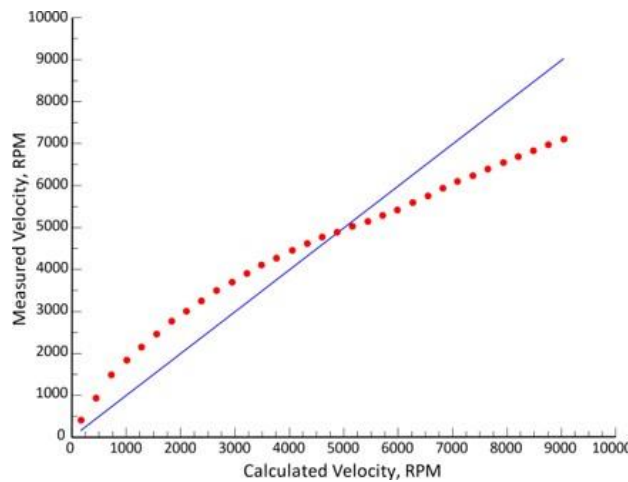


Figure 10. Rotational velocity: directly measured vs. calculated from model (2). Notations: blue line is the ideal relation if no uncertainties are present. red line is the results of measurements.

B. Performance of Propellers

Thrust generated by four propellers with untreated blades at different rotational speeds is shown in Fig. 11a. The propeller with the bio-inspired blades that have the NACA 64(4)-221 profile became unbalanced and further experiments were terminated after approximately 1300 RPM for safety reasons. The other three propellers were also slightly unbalanced and shaking at lower speeds. However, when the speed was increased, they were running smooth. Figure 11a demonstrates that both propellers with untreated rectangular blades create more thrust than the propeller with the bio-inspired blades, particularly, at higher rotational speeds above 4000RPM.

The current drawn from the motor versus the thrust generated is shown in Fig. 11b for the three propellers. Results are somewhat similar for all propellers. At higher-thrust operation, an advantage of using rectangular blades is less obvious with respect to the propellers efficiency, particularly when rectangular blades have the NACA 64(4)-221 profile.

From the results of testing propellers with untreated blades, we concluded that the symmetrical blade profile NACA0015 seems to be more efficient in the given experimental setup. Therefore, only propellers with the NACA0015 profile of the blades were treated and tested further.

Figure 12a compares results of testing the propeller with the rectangular blades, treated and untreated. In the figure, results for treated blades are shown after 1st, 3rd, and 5th treatments. Since treatment smoothes the blade surface, improvement in the propeller performance after the blades treatment was expected. What is interesting though is that the propeller seems to perform the best after the first treatment. However, results for this case are also less consistent, which is caused by the propeller being more unbalanced than at higher speeds. This leads to higher oscillations in measured values of the thrust and the current output at the same voltage input. Another interesting fact is that this

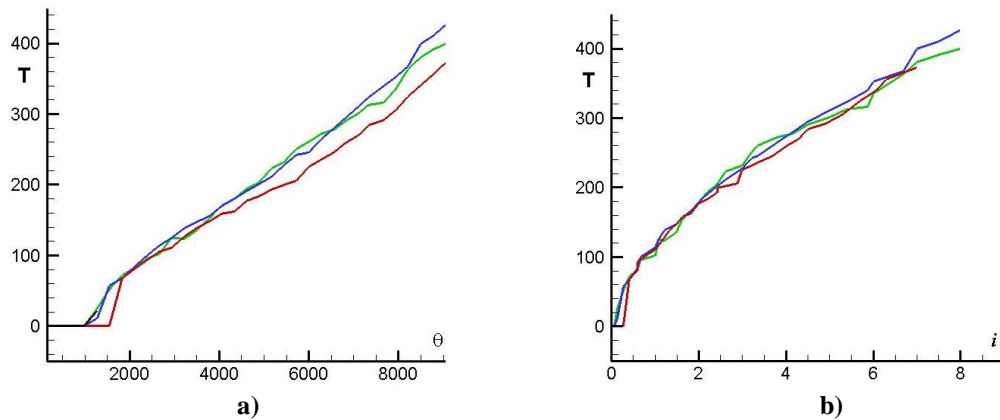


Figure 11. Performance of untreated propellers a) thrust (in gram-force) vs. rotational speed (in RPM), b) thrust vs. current. Color scheme for the propeller blades: green NACA64(4)-221 rectangular, blue NACA0015 rectangular, red NACA0015 bio-inspired, black NACA64(4)-221 bio-inspired.

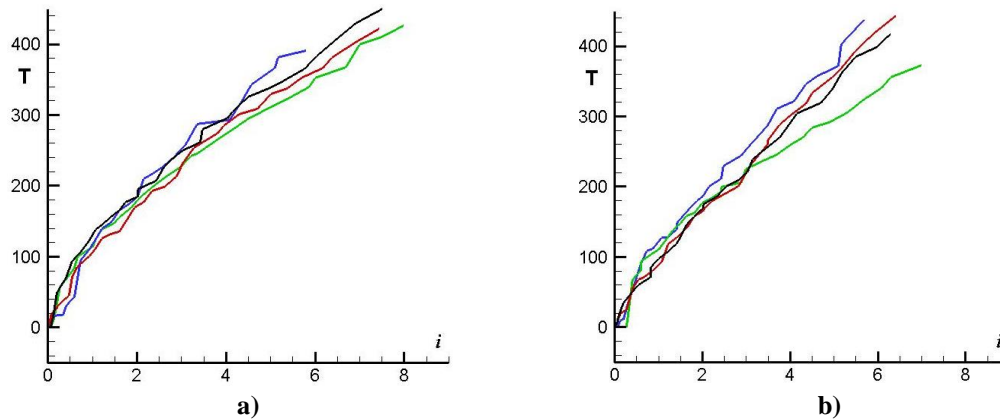


Figure 12. Performance of the propeller with the NACA0015 profile, a) rectangular blades, b) bio-inspired blades. Color scheme for the blades: green untreated, blue after the 1st treatment, red after the 2nd treatment, black after the 3rd treatment.

propeller produces the maximum thrust after the fifth treatment, even though the blade area is reduced and the blade surface is deteriorated the most in this case due to the blade treatment.

Results for the propeller with bio-inspired blades are shown in Fig. 12b. Similar to the propeller with rectangular blades, the blade treatment, and particularly, the first treatment has a beneficial effect on the performance of this propeller. Increasing a number of treatments is beneficial for the maximum value of the thrust that the propeller can produce. The maximum thrust generated by this propeller is ~450 gram-force, which is obtained after the third treatment of the blades. This value is close to the maximum thrust generated by the propeller with rectangular blades after the fifth treatment.

To compare the performance of two propellers, all results for untreated and treated blades were averaged for each propeller. The average thrust values are shown in Fig. 13. For the current draw of 3 amps and below, the results are almost identical for the two propellers. However, when the motor draws more than 3 amps, that is, at higher-thrust operation, the propeller with bio-inspired blades operates more efficiently. Although the maximum thrust value is at ~350 gram-force for both propellers, the propeller with bio-inspired blades draws approximately 1 amp less than the propeller with rectangular blades. At the draw of 5 amps, the propeller with bio-inspired blades is ~20% more efficient than the propeller with rectangular blades.

Results presented in Figs. 11-13 were obtained with model (2) for the rotational velocity. To verify whether a choice of a motor model affected the results of comparison of the two propellers performance, tests were repeated for the two propellers with the NACA 0015 blade profile after the 6th treatment using an EXTECH 461893 digital optical tachometer to measure the rotational velocity.

Figure 14 presents measured values of thrust as a function of the measured rotational velocity for both propellers. Results are only given for the thrust values higher than the propeller weight. The figure shows that indeed the propeller with the rectangular blades generates higher thrust at a given rotational velocity. For example, at close measured rotational velocities, the propeller with rectangular blades generated 2.91N (at $\theta = 7147$ RPM), but the propeller with bio-inspired blades produced 2.35N (at $\theta = 7134$ RPM), which is about 20% difference. The thrust profiles for both propellers qualitatively agree with the results obtained in [14-17] for quadrotor-type propellers.

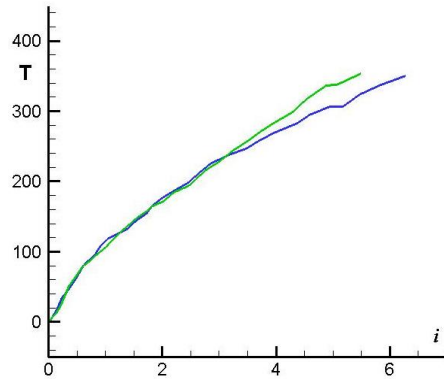


Figure 13. The propeller performance averaged over the blade treatments data: blue rectangular blades with the NACA0015 profile, green bio-inspired blades with the NACA0015 profile.

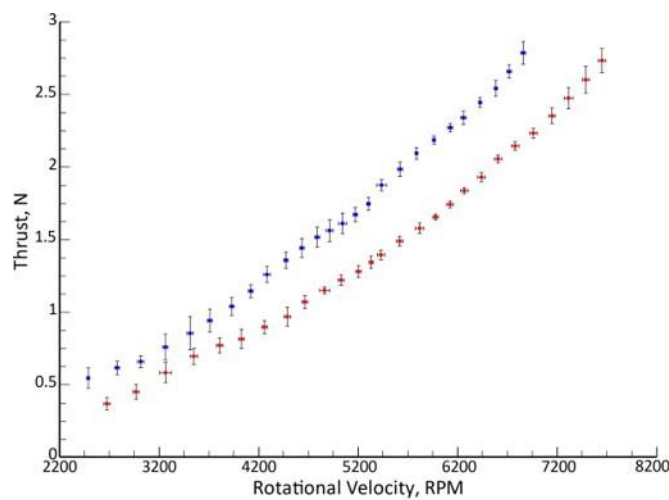


Figure 14. Thrust vs. rotational velocity for the propellers with the NACA0015 blade profile after the 6th treatment. Notations: blue dots – propeller with rectangular blades; red dots – propeller with the bio-inspired blades.

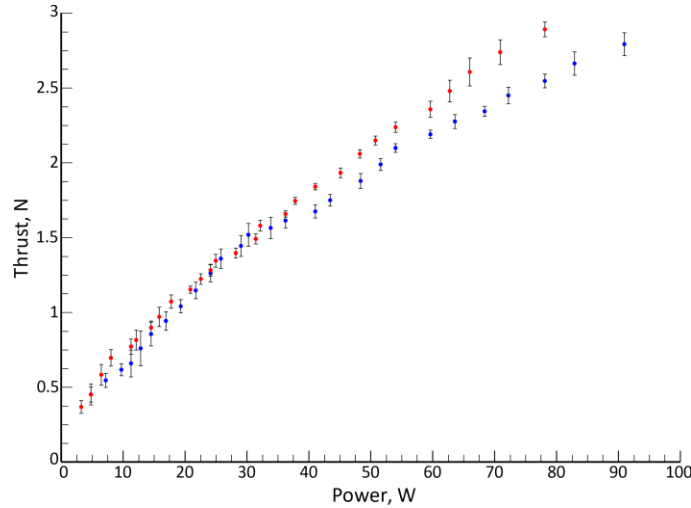


Figure 15. Thrust vs. power for blades after 6th treatment and with NACA 0015 airfoil. Notations are the same as in Fig. 14.

Other important characteristic is how thrust varies with respect to the power supply. These results for the two propellers are shown in Fig. 15. The figure demonstrates that the propeller with bio-inspired blades produces equal or more thrust than the one with rectangular blades for a given power supply. For example, at the maximum control input of 9000 RPM, which corresponds to supplied power of 78.12W (draws 6.51A) for the propeller with bio-inspired blades, the propeller thrust is 2.89N. For the same power supply, thrust of the propeller with rectangular blades is 2.54N, that is, 13.5% less.

Notice also that the measured rotational velocity of the propeller with bio-inspired blades is 16.6% higher than that of the propeller with rectangular blades at the same power input. This may indicate lower drag of bio-inspired blades to compare with rectangular blades, which leads to less torque and therefore, enables the motor to rotate at higher velocities.

To assess uncertainty in the thrust measurements, each propeller was tested 9 times and in each test, the rotational velocity in the control input of the test set was varied in the range from 166 to 9000 RPM, first increasing θ , and then, decreasing its value back to the minimum. At each incremental step, thrust value was recorded. That is, there was 18 measurements of thrust corresponding to a given rotational velocity from the control input. The accuracy of each control input was verified with its direct measurement using the tachometer.

Overall, results presented in Figs. 14-15 lead to conclusions about the performance of propellers with different blade designs similar to those obtained from the analysis of Figs. 11-13. In this respect, we can infer that model (2) even though it gives less accurate estimates of the rotational velocity than its direct measurements, is an acceptable alternative for fast comparison of the performance of multiple propeller designs in user-friendly environment. For accurate assessment of the performance of an individual propeller, direct measurements or a more accurate model should be employed.

Here, we compare the performance of two propellers when used as rotors in hover analytically, by comparing their figures of merit ($FM = P_i/P_{act}$) at a given disc loading ($DL = T/A$) [3], where P_i is the induced power, P_{act} is the actual power, and A is the rotor disk area. Here, the induced power is estimated from the measured thrust using results from the momentum theory (as described in [3]):

$$P_i = \frac{T^{3/2}}{\sqrt{2\rho A}}$$

The actual power supplied to a rotor, P_{act} , is assumed to be equal to electrical power supplied to a propeller in the experiments: $P_{act} = V * i$. Efficiency of ESC and that of the motor are not taken into account in the actual power calculations, because they are the same for both propellers and thus, will not change the results of comparison of the two propellers performance. Disc loading is based on the propeller diameter.

The figure of merit for the two propellers is presented in Fig. 16 as a function of disk loading. The figure demonstrates that the propeller with bio-inspired blades has a higher hover efficiency than the one with the rectangular blade at all considered values of the disk loading.

V. Conclusion

The paper presents results of the experimental testing of small 3D printed propellers with rectangular and bio-inspired blades, which have symmetrical (NACA0015) or asymmetrical (NACA 64(4)-221) profiles. Tests were conducted with propellers, which were untreated or chemically treated after manufacturing.

The asymmetrical blade profile was deemed unfavorable in our experimental setup. Only the propellers with the NACA0015 blade profile were chemically treated and their performance tested against each other. Chemical treatment has a beneficial effect on the performance of 3D printed propellers, with the first treatment showing the strongest effect. The effect of treatment on the propeller with bio-inspired blades is stronger. Treating propellers more than 3 times is not recommended for practical purposes.

Tests demonstrated advantages of using rectangular blades when comparing the thrust values at the same rotational speed. However, when considering the amount of thrust generated at a given power supply, bio-inspired blades are more efficient. The figure of merit estimated for a hovering rotor with the bio-inspired blades is also higher to compare with the one with rectangular blades at a given disk loading. The bio-inspired blade also seems to have less drag than the rectangular blade with the same planform area and profile. This has to be investigated further.

The accuracy of the linear motor model connecting the rotational speed and voltage supplied to a motor based on the motor Kv rating, was assessed. It was found that such a model is acceptable for comparison propellers of different designs, but accurate assessment of the individual propeller performance would benefit from either direct measurements of the rotational speed or a more advanced model for this parameter.

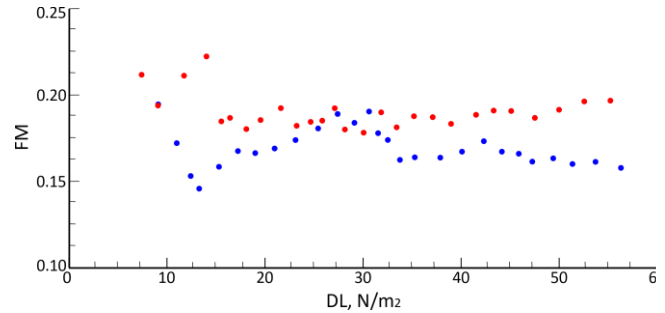


Figure 16. Figure of Merit vs. disk loading for the propellers with the NACA0015 blade profile after the 6th treatment. Notations are the same as in Fig. 14.

Acknowledgments

3D printing of the propellers was performed by Jason Church, Senior Machinist at the Prototype Machine Shop of the Department of Mechanical Engineering, University of New Mexico. CAD models of the blades were created by Lucca A. Henrion and Scott K. Garner, undergraduate students at the Department of Mechanical Engineering, University of New Mexico. Dassault Systèmes provided SolidWorks for academic purposes. The high-resolution Nikon DF camera used in making photographs was provided for this research by Prof. P. Vorobieff (Department of Mechanical Engineering, University of New Mexico).

References

- [1] Gomez, S., Gilkey, L. N., Kaiser, B. E., Poroseva, S. V., "Computational analysis of a tip vortex structure shed from a bio-inspired blade," AIAA2014-3253.
- [2] Handy, C., "Nature-inspired Rotorcraft Blade Design," M.S. Project Report, Mechanical Engineering Dept., University of New Mexico, Albuquerque, NM, 2012.
- [3] Leishman, J. G., *Principles of Helicopter Aerodynamics*, 2nd ed., Cambridge University Press, New York, 2000, Ch. 2, 7, 10.
- [4] Stratasys, Inc., *Modeling apparatus for three-dimensional objects*, US Patent 5340433 A, 1994.
- [5] Startasys, <http://www.stratasys.com/>
- [6] Garg, A. B., "Chemical vapor treatment of ABS parts built by FDM: Analysis of surface finish and mechanical strength," *The Int. J. Advanced Manufacturing Technology*, 89(5-8), 2175-2191, 2017.
- [7] Williams, R. E. (1998). Abrasive flow finishing of stereolithography prototypes. *Rapid Prototyping Journal*, 4(2), 56-67.
- [8] Kulkarni, P. "On the integration of layered manufacturing and material removal processes," *J. Manufacturing Science and Engineering*, 122(1), 100-108, 2000.
- [9] Pandey, P. M. "Improvement of surface finish by staircase machining in fused deposition modeling," *J. Materials Processing Technology*, 132(1), 323-331, 2003.
- [10] Espalin, D. M. (2009). Vapor Smoothing, A Method for Improving FDM-Manufactured Part Surface Finish. *International Rep. of the WM Keck Center for 3D Innovation*.

- [11] Galantucci, L. M. (2009). Experimental study aiming to enhance the surface finish of fused deposition modeled parts. *CIRP Annals-Manufacturing Technology*(58(1)), 189-192.
- [12] Galantucci, L. M. (2010). Quantitative analysis of a chemical treatment to reduce roughness of parts fabricated using fused deposition modeling. *CIRP Annals-manufacturing technology*(59(1)), 247-250.
- [13] DC Motor Speed: System Modeling.
<http://ctms.engin.umich.edu/CTMS/index.php?example=MotorSpeed§ion=SystemModeling>
- [14] Kotwani, K., Sane, S., Arya, H., & Sudhakar, K. (2004). Experimental Characterization of Propulsion System for Mini Aerial Vehicle. *31 National Conference on FMFP*. Kolkata.
- [15] Brezina, A., & Thomas, S. (2012). Measurement of Static and Dynamic Performance Characteristics of Electric Propulsion Systems. *51st AIAA Aerospace Sciences Meeting including the New Horizons Forum and Aerospace Exposition*. Dallas, Texas.
- [16] Intaratep, N., Alexander, W. N., Devenport, W. J., Grace, S. M., & Dropkin, A. (2016). Experimental Study of Quadcopter Acoustics and Performance at Static Thrust Conditions. *22nd AIAA/CEAS Aeroacoustics Conference*. Lyon, France.
- [17] Smedresman, A., Arbor, A., Yeo, D., & Shyy, W. (2011). Design, Fabrication, Analysis, and Dynamic Testing of a Micro Air Vehicle Propeller. *29th AIAA Applied Aerodynamics Conference*. Honolulu, Hawaii.